Numerical simulation of the non-Newtonian blood flow through a mechanical aortic valve: Non-Newtonian blood flow in the aortic root

(Article begins on next page)

10 April 2024

Numerical simulation of the non–Newtonian blood flow through a mechanical aortic valve

Non–Newtonian blood flow in the aortic root

F. De Vita

DII, Università di Roma 'Tor Vergata', Italy.

M.D. de Tullio

DMMM, Politenico di Bari, Italy.

R. Verzicco

DII, Università di Roma 'Tor Vergata', Italy & PoF, University of Twente, The Netherlands.

Abstract. This work focuses on the comparison between Newtonian and non–Newtonian blood flows through a bileaflet mechanical heart valve in the aortic root. The blood, in fact, is a concentrated suspension of cells, mainly red blood cells, in a Newtonian matrix, the plasma, and consequently its overall behavior is that of a non–Newtonian fluid owing to the action of the cells' membrane on the fluid part. The common practice, however, assumes the blood in large vessels as a Newtonian fluid since the shear–rate is generally high and the effective viscosity becomes independent of the former. In this paper we show that this is not always the case even in the aorta, the largest artery of the systemic circulation, owing to the pulsatile and transitional nature of the flow. Unexpectedly, for most of the pulsating cycle and in a large part of the fluid volume, the shear–rate is smaller than the threshold level for the blood to display a constant effective viscosity and its shear–thinning character might affect the system dynamics. A direct inspection of the various flow features has shown that the valve dynamics, the transvalvular pressure drop and the large–scale features of the flow are very similar for the Newtonian and non–Newtonian fluid models. On the other hand the mechanical damage of the red blood cells (haemolysis), induced by the altered stress values in the flow, is larger for the non–Newtonian fluid model than for the Newtonian one.

1. Introduction

Cardiovascular disorders are nowadays the leading cause of death in developed countries and the related health and economic issues have lead to a number of devices and surgical techniques for their treatment (Guccione, 2010). Examples of such devices range from coronary stenting for stenoses up to the total artificial heart. Among many others, valvular heart diseases have a relevant incidence (Votta, *et al*., 2013) and this has motivated the need for major improvements in the artificial valves as well as in the surgical repair and implantation techniques. The human heart has four valves since it consists of two pumps (right

and left) each one with two chambers: the right heart pumps the blood to the pulmonic (small) circulation and it provides about 30 mmHg of maximum pressure difference. The left heart, on the other hand, feeds the systemic (large) circulation that needs no less than 90–100 mmHg to work properly. The valves ensure that the blood flows only in one direction by opening during the forward– and closing at the beginning of the back–flow thus minimizing the blood regurgitation and maintaining the pumping efficiency. Because the valves of the left heart have to withstand the largest pressure differences they are more subject to damage and the aortic one is affected more frequently (Carrel, *et al.*, 2013).

Numerical simulations of the blood flow through the functional unit aortic root/aortic valve are becoming a precious tool to improve surgical techniques and the performance of prosthetic devices. A computational model for the complete system is therefore driven by physical, physiological and economic motivations; sufficiently accurate computational models, in fact, would serve as inexpensive tools for scientific and medical research that, combined with medical imaging and other cardiovascular diagnostic techniques, would provide fundamental information for the improvement of the patients care (Marsden, 2013). In fact, numerical simulations allow the measurement of potentially any primitive or derived quantity that would be prohibitive in *in vivo* or even *in vitro* tests, they permit the proof of concept of innovative technologies and, in the near future, they could be used for patient–specific diagnoses or surgical planning.

On the other hand, the reliability of numerical simulations depends either on the quality of the numerical method and on the fidelity of the physical model; among the challenges of the former there is the wide range of spatial and time flow scales, the intrinsic unsteady nature of the problems and the demanding computational techniques. The physical model, on the other hand, describes the geometry of the system, the properties of solid materials, their interactions with the flow and also the constitutive relation for the fluid. Concerning the latter, in the literature, the common belief is that the blood behaves as a Newtonian fluid in large vessels (Siginer, 1999), since its effective viscosity becomes asymptotically constant for high shear–rates. In the aorta, the largest artery, this assumption is taken for granted and all the studies rely on the Newtonian fluid model where the viscosity is constant and independent of the deformation–rate. Looking at (Siginer, 1999), however, it appears that this conjecture is based on the hypothesis of a steady laminar flow within a rigid cylindrical domain (Hagen-Poiseuille flow). In reality, the blood flow in the aortic root is pulsatile and transitional (or even turbulent) which implies that the previous assumption might not be correct.

In this paper we show, by direct numerical simulations, that indeed it is the case and using a non–Newtonian (shear thinning) fluid model yields quite different results for the phenomenon of haemolysis. On the other hand, other features like the dynamics of the mechanical valve or the transvalvular pressure drop remain basically unchanged regardless of the fluid model.

2. The Model

The computational set–up is that sketched in Figure 1 with a Sorin Bicarbon bileaflet mechanical valve in a physiological aortic root with three Valsalva sinuses similarly to what simulated in (de Tullio, *et al.*, 2009). The geometry of the aortic root exactly reproduces the model used in (de Tullio, *et al.*, 2009) and it closely corresponds to the physiological case: at the outlet of the valve, the three sinuses of Valsalva are placed at equispaced radial positions. The valve is mounted in an intra-annular configuration, meaning that the valve housing does not extend into the sinuses of Valsalva, and in an asymmetric orientation with respect to the sinuses. A flow is prescribed according to the time law of Figure 2 through the circular section of diameter $d = 2.5$ cm that is also the main scaling length. The fluid flow produces hydrodynamic loads that cause the motion of the two leaflets hinged at the frame of the valve (dark gray element of Figure 1). The time–dependent position of the leaflets, in turn, determine the geometry of the fluid domain and therefore the flow. These problems, where fluid and structure influence each other are referred to as fluid/structure interaction problems (FSI) and they need the solution of the fluid and the structural part in a coupled way. Details of the solution procedure can be found in (de Tullio, *et al.*, 2009) here it suffices to mention that the Navier–Stokes equations

$$\frac{D\mathbf{u}}{Dt} = -\nabla p + \frac{1}{Re}\nabla \cdot [2\nu(\mathbf{E})\mathbf{E}] + \mathbf{f}, \qquad \nabla \cdot \mathbf{u} = 0 \tag{1}$$

and the equilibrium to rotation of the leaflets

$$I_i \frac{d^2\theta_i}{dt^2} = T_i, \qquad \text{with} \qquad i = 1, 2 \qquad \text{and} \qquad T_i = \int_{S_i} [(\tau \cdot \mathbf{n} - p\mathbf{n}) \times \mathbf{r}] \cdot \hat{x} \mathrm{d}S \qquad (2)$$

are solved iteratively using a predictor–corrector method. Here D/Dt is the material derivative, $\mathbf{u}$ and p, respectively, velocity vector and pressure and $\mathbf{E} = [\nabla \mathbf{u} + (\nabla \mathbf{u})^T]/2$ the symmetric part of the velocity gradient tensor. $\mathbf{f}$ is the body force term used to enforce the no–slip velocity boundary condition on the complex geometry within the immersed boundary context as described by Vanella and Balaras (2009). I_i is the moment of inertia of the i–th leaflet and θ_i its angular position. T_i is the moment of the hydrodynamic loads with respect to an axis passing through the hinges (whose unit vector is $\hat{x}$).

The set–up of figure 1 is 'immersed' in a Cartesian structured grid having $262 \times 181 \times 181$ nodes in the streamwise and cross–stream directions, respectively. The nodes have been distributed non uniformly so that they are mainly clustered in the region of the valve and its wake that need more spatial resolution. The geometry of the valve is a perfect copy of the real one except for the hinge that, being very sophisticated, would deserve a dedicated investigation. Here, following (de Tullio, *et al*., 2009), it has been modeled by a gap of 0.15 mm width in which five computational nodes have been clustered in order to describe the crossing flow. This spatial resolution has already been checked in other papers (de Tullio, *et al*., 2009) against grid–refinements checks to be adequate to resolve all the flow scales for the Reynolds number (later defined) of this problem.

The incompressible NavierStokes equations are discretized in space using second–order–accurate central differences in conservative form. The resulting system is inverted using a fractional–step method, where the viscous terms are computed implicitly and the convective terms explicitly ((Verzicco and Orlandi, 1996)). All the simulations have been run with a fixed Courant number $CFL = 0.25$, thus having a variable time step Δt which is dynamically adjusted during the cycle. The time integration procedure employs a very high temporal resolution; in this case the time spacing ranged from 2 to 200 μs during a cardiac cycle. A strong fluid–structure–interaction coupling, in which equations (1–2) are solved together through an iterative procedure, is required to ensure stability and robustness of the simulation over the whole cardiac cycle owing to the high acceleration of the leaflets. This is necessary because the added mass effects are relevant in the valve dynamics and a 'loose coupling' approach, in which the two systems are integrated separately, would diverge ((Borazjani , *et al*.,2008)). More details on the method are given in (de Tullio, *et al*., 2009).

Concerning the added mass it is worth mentioning that, being forces and momenta computed through the surface integrals (2), its effect is already accounted in those expressions being the pressure and viscous stress distribution over the leaflet surface determined also by the inertia of the displaced fluid. On the other hand, if the leaflets dynamics were computed by force and moment coefficients (determined from steady flows) the added mass effect would need to be considered.

Ten complete cardiac cycles are simulated and the results are phase averaged. The assumed cardiac output is about 5 l/min at a fixed beat rate of 70 beats/min, resulting in a stroke volume of about 72 ml. The blood density is set to $\rho_b = 1060$ kg/m^3. The peak Reynolds number, based upon the bulk velocity at the peak inflow, $U = 1.2$ m/s, the inflow tube diameter, and the asymptotic blood kinematic viscosity $\nu_\infty = 3.7 \times 10^{-6}$ m^2/s, is about $Re = 6800$.

Further details about the numerical values of the various quantities and material properties can be found in (de Tullio, *et al*., 2009) and (de Tullio, *et al*., 2012); the only relevant difference is that here the kinematic viscosity of the fluid can be either a constant $\nu(\mathbf{E}) = \nu_0$ or a function of the rate–of–strain tensor $\mathbf{E}$. In the first case the fluid is Newtonian, in the second is non-Newtonian.

Among the various possibilities we have adopted for the blood the shear–thinning model of Carreau–Yasuda (Siginer, 1999) that reads

$$\nu(\mathbf{E}) = \nu_\infty + (\nu_0 - \nu_\infty)[1 + (\lambda E)^2]^{(n-1)/2} \qquad (3)$$

where $E = | \mathbf{E} |$ is the norm of the rate–of–strain tensor and both λ and n are hematocrit dependent parameters. We have chosen the parameters for an adult healthy male with an hematocrit of 40% that yield $\nu_\infty \simeq 3.7 \times 10^{-6}$ m^2/s for high shear rates and $\nu_0 \simeq 4.3\nu_\infty$ for vanishing shear rates.
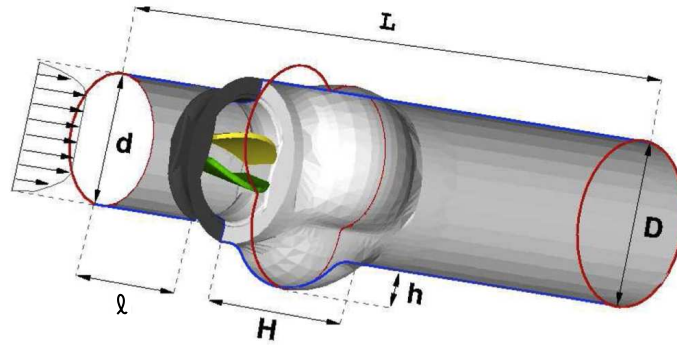
Figure 1. Sketch of the computational set–up. Main lengths: $D = 1.26d$, $\ell = d$, $L = 5d$, $H = 1.14d$, $h = 0.26d$.
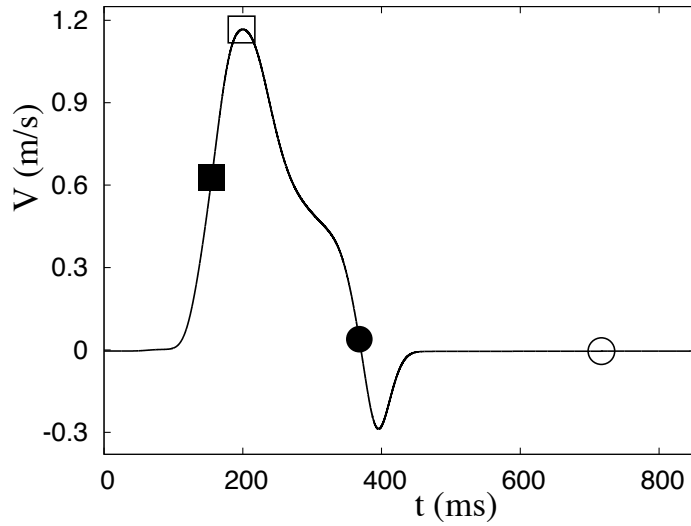

Figure 2. Mean axial velocity during the flow cycle. The symbols identify: valve fully open (filled square), peak flow (open square), valve closed (bullet) and flow settling (open circle). The same symbol meaning will be maintained through the paper.

3. Results

3.1. Preliminary Considerations

In (de Tullio, *et al.*, 2012) a Newtonian fluid model was used to study the haemolysis produced by a bi–leaflet mechanical aortic valve in physiological conditions. All the flow conditions were the same as those described in the previous section with the left ventricular volume ejection as that of an adult human male at rest (heart beat 72 beats/min). The curve of the volume flux time evolution looks like in Figure 2 where some representative instants during the cycle have been evidenced by symbols. The inflow of Figure 2 results in a peak Reynolds number of about 6800 that is indeed the physiological value. Using the data of that study, for each of the four characteristic phases of the cycle the modulus of the rate–of–strain tensor **E** has been computed from the instantaneous three–dimensional velocity field in *each* point of the domain and its probability distribution function (pdf) computed. Since the flow is pulsatile the pdfs have been phase averaged over 10 cycles although already a couple of cycles yielded converged statistics. The results are shown in Figure 4 and they clearly show that none of the shear rate distributions supports the hypothesis
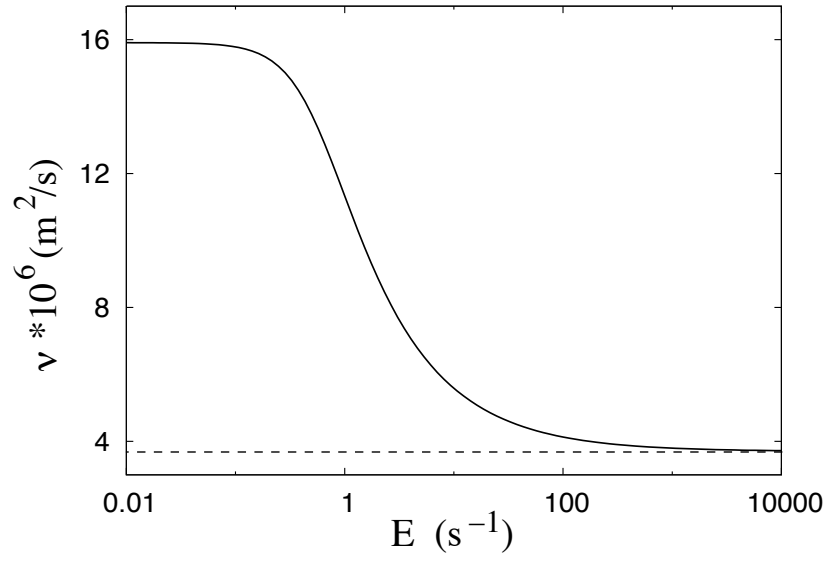
Figure 3. Variation of the kinematic viscosity ν as function of the shear rate norm E, according to the relation (3), for an hematocrit of 40%. The horizontal dashed line is the value ν_∞ used for the Newtonian simulation.

of fluid with constant viscosity; this is not even true for the pdf computed at the flow peak instant of the cycle where the velocities are the highest and the shear rates more intense.
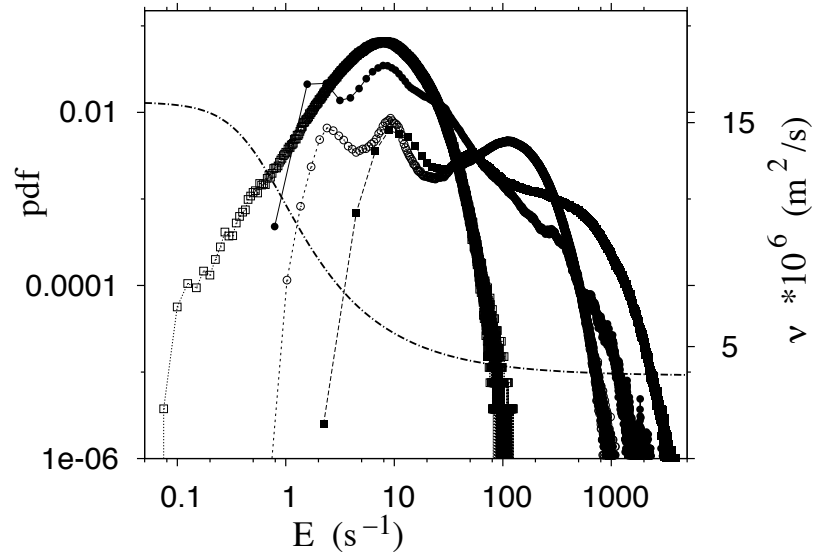

Figure 4. Probability distribution functions of the shear rate for 4 representative instants in the cycle for the Newtonian fluid model. The pdfs are overlaid onto a curve for the shear rate dependence of the blood viscosity (hematocrit 40%). Symbols as in Figure 2.

Looking at instantaneous snapshots of the flow (Figure 5) this result is not surprising since the high shear rate regions look very localized in space and there are several recirculations and laminar pockets where

the shear rates are reduced. In addition from Figure 2 it is evident that for more than 60% of the cycle the flow rate is nearly zero and the incipient turbulence that has bursted during the decelerating part of the cycle (with an adverse pressure gradient) gradually settles down because of viscosity. In this scenario, the dynamics is clearly dominated by the low shear rates regions and a non–Newtonian fluid model is more appropriate. These considerations are the main motivation for the present study.
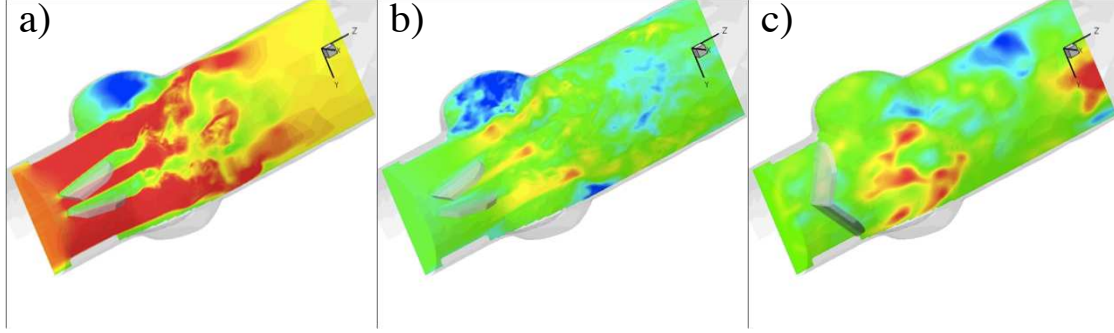

Figure 5. Instantaneous snapshots of axial velocity through a central symmetry plane at three instants of the cycle for the Newtonian fluid model: a) peak flow, b) valve closing and c) flow settling. (red maximum values, blue minimum values).

3.2. Non–Newtonian fluid simulations

The simulations described above have been repeated using the shear thinning relation (3) and some results are reported and discussed below. A first important finding is that the dynamics of the leaflets (in terms of positions in time and velocities of opening and closing) is essentially unaffected by the non-Newtonian fluid model as shown by the results of Figures 6. This is due to the fact that the largest contribution to the moments T_i of equations (2) is given by the pressure term while the viscous part is generally negligible. Direct evidence of this statement is given in Figure 7 showing the separate contributions of the pressure and viscous stresses contributions, M_p and M_ν respectively (in non-dimensional units), to the moments of equation (2). For the same reason, also the transvalvular pressure drop (which in fact is the overhead paid by the heart) shows negligible differences for the two fluid models, with a peak value of 1600 Pa ($\simeq 12$ mmHg) and a mean systolic value of 490 Pa ($\simeq 3.7$ mmHg) in both cases.

The pdfs of the shear rate and the instantaneous snapshots of Figures 9 and 10, on the other hand, show some differences either in the structure of the large–scale flow and in the relative importance of large– and small–scales. The latter are particularly relevant for the phenomenon of haemolysis that is the permanent damage of a red blood cell owing to a combination of high levels of shear rates and long exposure times.

In this paper we have quantified these factors by the Haemolysis Index (HI) (Goubergits and Affeld, 2004), as the ratio of the increase of the plasma-free hemoglobin concentration ($dPHb$, in mg/100 ml) after mechanical loading to the total hemoglobin concentration (Hb, in mg/100 ml): $HI = 100 \cdot dPHb/Hb(\%)$. This model has been implemented in our calculations using a Lagrangian approach that allows to account for the exposure time to a given stress level. More in detail, 4×10^5 'fluid particles' are tracked as they flow into the system, and HI is estimated along each trajectory by evaluating the total damage accumulated in time. This requires a modifications of the above equation in order to improve its accuracy in unsteady flow environments. In particular, the model proposed by (Giersiepen, *et al.*, 1990) defines $\Delta HI_i = \alpha C t_i^{\alpha-1} \tau(t_i) \Delta t_i$ (with $C = 3.62 \times 10^{-5}$, $\beta = 2.416$ and $\alpha = 0.785$ for red blood cells) as the incremental haemolysis index accumulated at time t_i over a time interval Δt_i because of an exposure to a stress τ. It is worthwhile mentioning that in this analysis we have not introduced Lagrangian particles in the flowfield instead we have only tracked in a Lagrangian way *fluid particles*; these are not single red blood cells but rather small elements of fluid still considered as a continuum phase. These particles, therefore, do not need to be coupled neither one–way nor two–way with the flow since they *are* the flow. In other words starting from selected initial control points we integrate the equation $\dot{\mathbf{x}}(t) = \mathbf{u}(\mathbf{x}, t)$ that gives the trajectory of the fluid particles
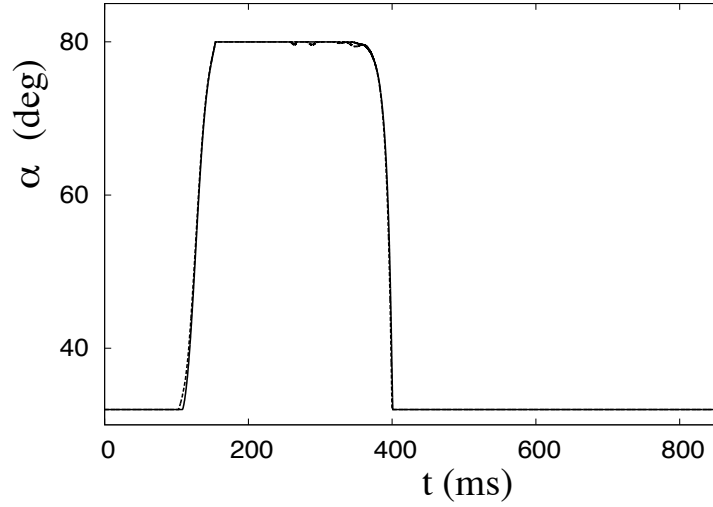
Figure 6. Angular position of the upper leaflet of the mechanical valve during the flow cycle: solid line for the Newtonian fluid model, dashed line for the non–Newtonian fluid model.

Figure 7. Time evolution of the pressure (a) and viscous (b) moments about the hinge for the upper leaflet of the mechanical valve during the flow cycle: solid line for the Newtonian fluid model, dashed line for the non–Newtonian fluid model.
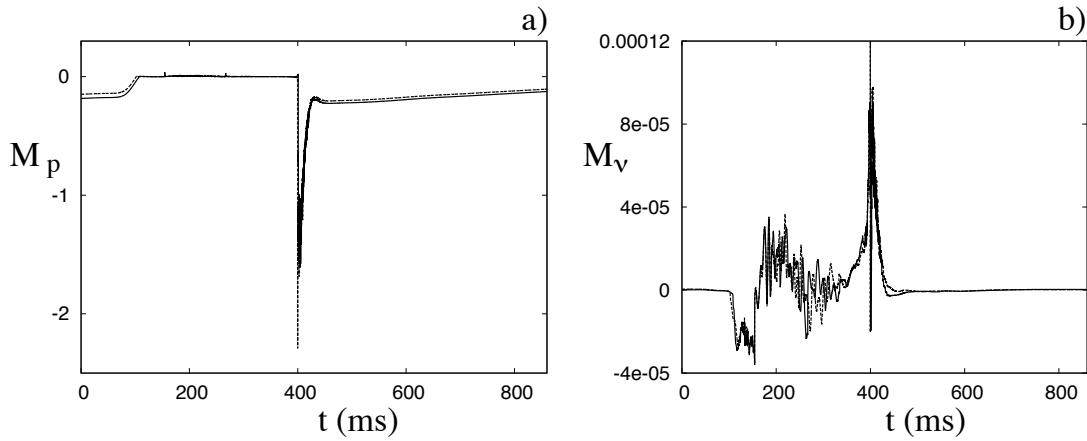
over which we can compute the damage accumulated by the red blood cells contained in the fluid particle from the knowledge of the stress level along the trajectory and the exposure time to that stress.

In complex flow fields, defining the scalar quantity, τ, is not trivial since the stress is a tensor and it is strongly dependent on space and time. An interesting method has been proposed in (Arora *et al*. 2004), where the deformation of red blood cells is directly considered. In particular, red blood cells are assumed to behave like neutrally buoyant liquid droplets with defined physical properties. An evolution equation for a symmetric, positive definite morphology tensor, $\mathbf{S}$, whose square roots of eigenvalues and eigenvectors represent the half–axes of the ellipsoidal droplet, is solved (Maffettone and Minale, 1998). The equation reads:

$$\frac{\mathrm{d}\mathbf{S}}{\mathrm{d}t} = -(1 - f_2)(\boldsymbol{\Omega} \cdot \mathbf{S} - \mathbf{S} \cdot \boldsymbol{\Omega}) = -f_1[\mathbf{S} - g(\mathbf{S})\mathbf{I}] + f_2[\nabla \mathbf{u} \cdot \mathbf{S} + \mathbf{S} \cdot \nabla \mathbf{u}^T], \qquad (4)$$

where $g(\mathbf{S}) = 3III/II$ with III and II the third and the second invariant of the tensor $\mathbf{S}$, respectively, and $f_1 = 5.0 \ \mathrm{s}^1$, $f_2 = 4.2298 \cdot 10^4$ are model parameters calibrated to capture RBC–specific behavior. Equation (4) takes into consideration the competing action of interfacial tension on the droplet surface, which recovers the spherical shape of the droplet, and the force exerted by the surrounding liquid that tend
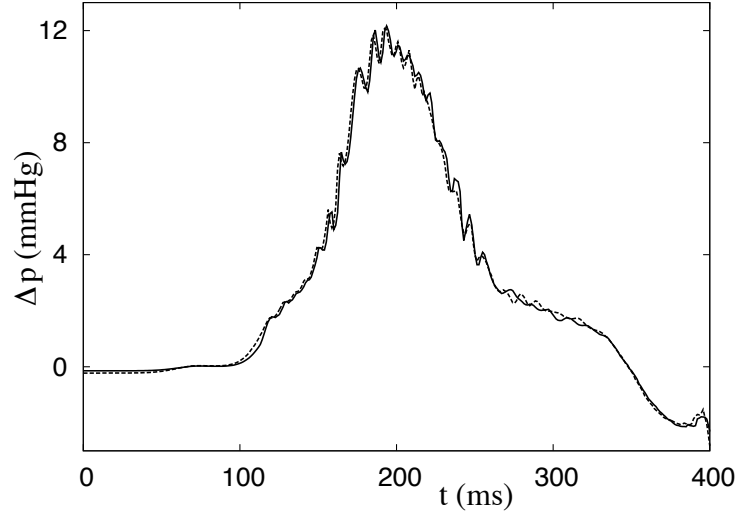
Figure 8. Systolic transvalvular pressure drop across the valve: solid line for the Newtonian fluid model, dashed line for the non–Newtonian fluid model.
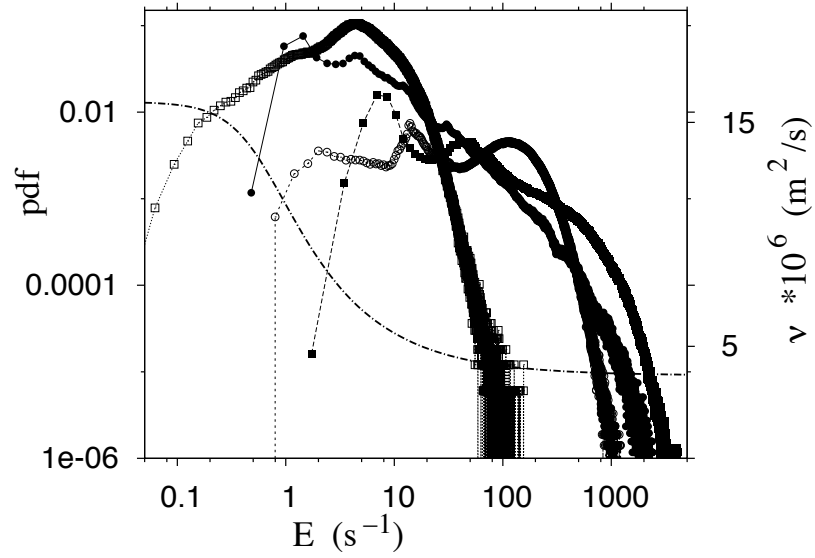

Figure 9. Probability distribution functions of the shear rate for 4 representative instants in the cycle for the non–Newtonian fluid model. The pdfs are overlaid onto a curve for the shear rate dependence of the blood viscosity (hematocrit 40%). Symbols as in Figure 2.

to deform it. All the details about the integration of equation (4) can be found in (de Tullio, *et al.*, 2012) here it suffices to mention that from history of **S** along each trajectory, the time evolution of the largest (L_i) and smallest (l_i) half–axes of each i–th ellipsoidal particle it can be computed together with the form factor $\Phi_i = (L_i - B_i)/(L_i + B_i)$ from which the strain is estimated as $\tau = \mu 2\Phi_i f_1/[(1 - \Phi_i^2)f_2]$ being μ the dynamic viscosity of the fluid and f_1 and f_2 the above defined constants used in equation (4).

The HI for each Lagrangian trajectory is then averaged among the tracers and phase averaged among the cycles so that a single evolution for each configuration has been obtained. The rationale for this averaging is that, as noted in (de Tullio, *et al.*, 2009), the life time of a red blood cell is 120 days and with a flow rate of 5 l/min and a total volume of blood of 5 l each red blood cell will cross the aortic valve about
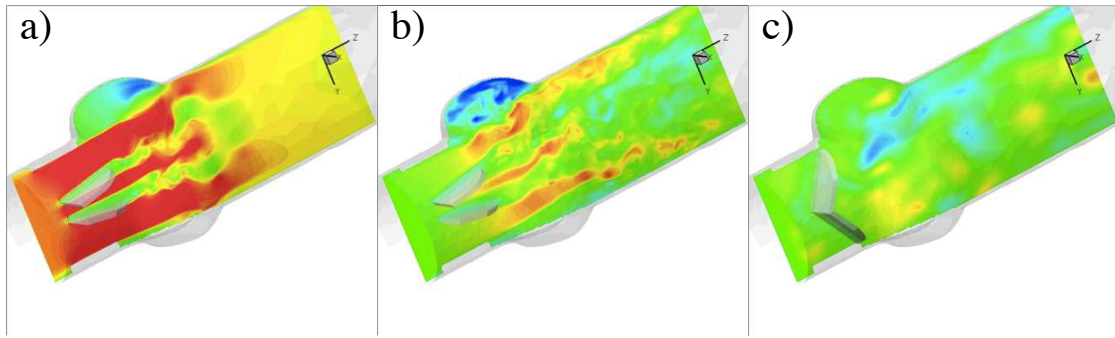
Figure 10. Instantaneous snapshots of axial velocity through a central symmetry plane at three instants of the cycle for the non–Newtonian fluid model: a) peak flow, b) valve closing and c) flow settling. (red maximum values, blue minimum values).

1.75×10^5 times; this implies that every cell is likely to experience every 'event' of the flow through the aortic valve and its HI can be accordingly obtained by and ensemble average of simultaneous events.

Figure 11 shows that the cycle evolution of the Haemolysis Index behaves in a very similar way in both cases although it is evident that the non-Newtonian fluid model yields a larger HI (larger damage) the difference being of the order of 17%. This is consistent with the results of figure 9 showing a stronger flow activity in the low shear–rate region where the non–Newtonian fluid has a larger viscosity.

We wish to stress that being HI computed from the fluid stress it depends on the viscosity model on two counts: I) Because different fluid models (Newtonian and non–Newtonian) produce different flow fields and II) because the calculation of the stress in the HI formula, for a given a flow field, also depends on the local value of viscosity. In order to separate these two effects we have also performed the computation of HI following an idealized procedure in which the flow field is computed using the Newtonian fluid model while the calculation of the haemolysis index relies on the non-Newtonian shear thinning model. The result is also reported in figure 11 and it is clear that the two effects are entangled since considering only one of them does not account for the total difference between Newtonian and non–Newtonian models.

This observation is reinforced by the curves of figure 12a showing that the viscosities themselves behave differently during the cycle and that even if the viscosity $\nu(\mathbf{E})$ were computed according to equation (3) but using the rate–of–strain tensor $\mathbf{E}$ coming from the simulation with the Newtonian fluid model, the results would not be the same.

It is interesting to note, finally, that the cycle averaged shear–rate experienced by the fluid particles for the non–Newtonian and Newtonian fluid models (figure 12b) do not differ much with the latter slightly bigger than the former as it could be guessed from the reduced viscosity. Nevertheless, when $\mathbf{E}$ computed from the Newtonian fluid simulation is plugged into the Carreau–Yasuda model (3) neither the HI nor the effective viscosity are correctly predicted. This is because the distribution of the shear–rate among the spatial scales turns out to be different for the two fluid models as is evident from the comparison of the probability distribution functions of figures 4 and 9. This suggests that, even if the increased HI predicted by the non–Newtonian fluid model could be recovered by an 'ad–hoc' increase of the ν_∞ viscosity of the Newtonian fluid model, this tuning would not have a general validity. In fact, each flow would have a different structure and a different share of small and large scales thus yielding different effective viscosities.

4. Conclusions

A series of direct numerical simulations of the blood flow through a mechanical bileaflet aortic valve, under physiologic conditions, have been performed using a Newtonian and a non–Newtonian (Carreau–Yasuda shear–thinning) fluid model.

Despite the common belief that the blood behaves as a Newtonian fluid in large vessels, the results have shown that the Newtonian fluid model might not be appropriate in all situations since the flow is very inhomogeneous in space and time. Even at the highest flow rate the zones of high shear–rates are very
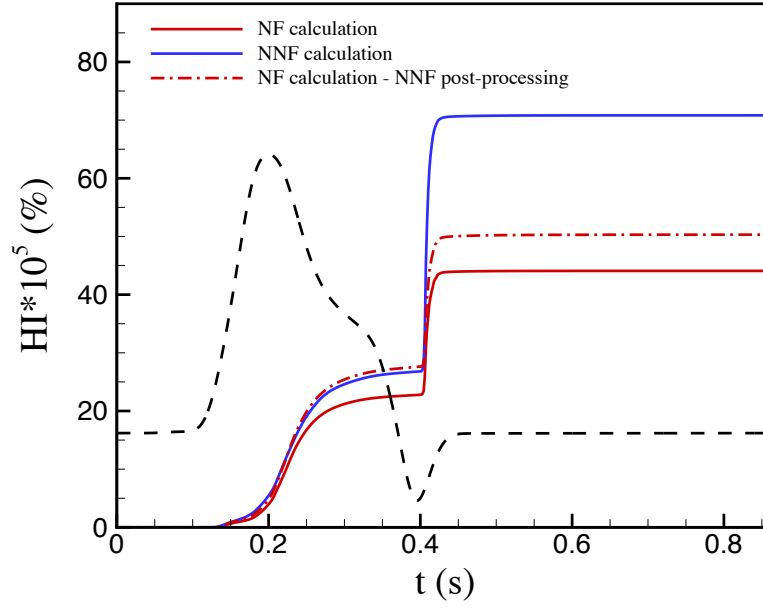
Figure 11. Time evolution of the HI for the non–Newtonian fluid (NNF) model (solid blue), the Newtonian fluid (NF) model (solid red) and NF simulation with NNF calculation of haemolysis (chaindot red).

Figure 12. *a)* Time evolution of the averaged viscosity felt by the fluid particles for the non–Newtonian fluid (NNF) model (solid blue), the Newtonian fluid (NF) model (solid red) and NF simula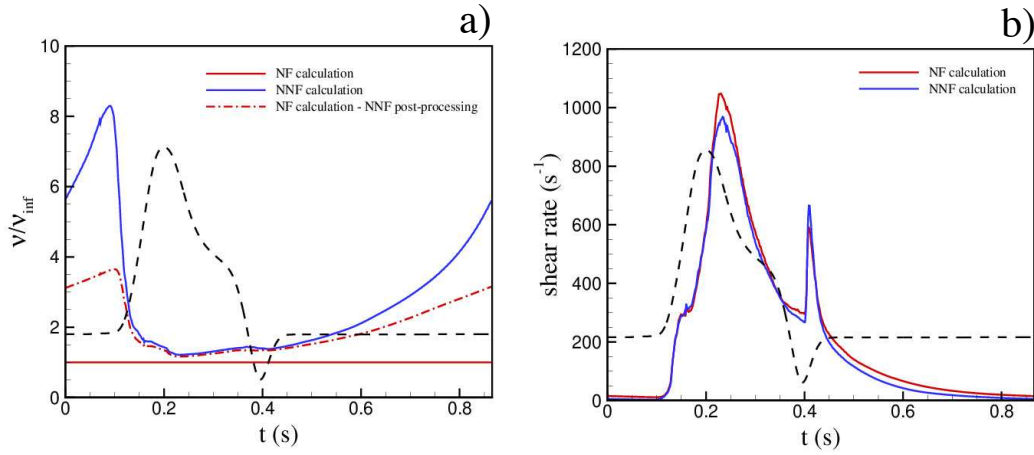tion with NNF calculation of haemolysis (chaindot red). *b)* Averaged equivalent shear–rate experienced by the fluid particles for the non–Newtonian fluid (NNF) model (solid blue) and the Newtonian fluid (NF) model (solid red).

localized in space while extended regions with recirculations or homogeneous flow are present. In addition, for most of the cardiac cycle the mean flow rate in the aortic root is zero and the flow is settling down thus producing low shear–rates.

A comparison of the results for the Newtonian and non-Newtonian fluid model, in otherwise identical conditions, has shown that the valve dynamics and the transvalvular pressure drop are hardly affected by the

fluid model while the haemolysis shows relevant differences. We can then conclude the indeed the blood in the aorta behaves as a Newtonian fluid for what concerns the dynamics of the valve and the large scale features of the flow. In contrast, the blood damage produced by the abnormal shear–rates induced by the mechanical valve is different with a value of the Haemolysis Index (HI) that is 17% bigger in the case of non–Newtonian fluid. These aspects and the final goal of the numerical investigation should be kept in mind when selecting the computational fluid model since the non–Newtonian fluid requires smaller time step sizes for the numerical integration of the equations and the simulation is about twice more expensive.

As correctly note by one Reviewer, a 17% variation of the haemolysis index might not be significant because there is a lot of uncertainty in the parameters for a non-Newtonian blood model and even for the structure of the model itself. Within this scenario the figures might be easily doubled of halved by a different blood model. The main claim of this paper, however, is not the specific HI variation but rather that the non–Newtonian character of the blood can have an effect on some aspects of the hemodynamics even in the aorta where the common belief is that the blood behaves as a Newtonian fluid.

As an aside we note that using a shear thinning model for the blood is only a first step towards more realistic simulations since the blood exhibits also viscoelastic properties and a model should account also for the time history of the rate of strain. This aspect has not be accounted yet and it might be the subject for a future study.

References

Guccione, J.M., Kassab, G. and Ratcliffe, M., *Computational Cardiovascular Mechanics* (Springer, Berlin 2010).

Votta, E. and Le, T.B. and Stevanella, M. and Fusini, L. and Caiani, E.G. and Redaelli, A. and Sotiropoulos, F., Journal of Biomechanics **46**, (2013), 217–228.

Carrel, T., Englberger, L. and Stalder, M., Open Journal of Cardiology **4**, (2013).

Marsden, A.L., Phys. of Fluids **25**, (2013), 101303.

Gijsen, F.J.H., Van de Vosse, F.N., *et al*., Journal of Biomechanics **32**, (1999), 601–608.

Siginer, D.A., De Kee, D. and Chhabra, R.P., *Advances in the flow and Rheology of non-Newtonian fluids* (Elsevier, Amsterdam 1999).

M.D. de Tullio, A. Cristallo, E. Balaras and R. Verzicco, J. of Fluid Mech. **622**, (2009) 259–290.

Vanella, M. and Balaras, E., J. Comput. Phys. **228**, (2009) 6617–6628.

de Tullio, M.D., Nam, J., Pascazio, G., Balaras, E. and Verzicco, R. Eur. J. of Mech. B/fluids **35**, (2012), 47–53.

Borazjani, I., Ge, L. and Sotiropolos, F. J. Comput. Phys. **227**, (2008), 75877620.

Verzicco, R. and Orlandi, P. J. of Comp. Phys. **123**, (1996), 402–414.

L. Goubergrits K. Affeld, Artif. Organs **28**, (2004) 499–507.

Arora, D., Behr, M. and Pasquali, M., Artif. Organs **28**, (2004) 1002–1015.

Maffettone, P. and Minale, C., J. of Non–Newt. Fluid Mech. **78**, (1998) 227–241.

Giersiepen, M., Wurzinger, L. J., Opitz, R., Reul, H., Intl J. Artif. Organs **13**, (1990) 300–306.